CHEMISTRY OF MATERIALS

Article

pubs.acs.org/cm

A Novel, Reactive Green Iron Sulfide (Sulfide Green Rust) Formed on Iron Oxide Nanocrystals

Christopher J. Jones,[†] Soma Chattopadhyay,[‡,§] Natalia I. Gonzalez-Pech,[†] Carolina Avendano,[†] Nina Hwang,[†] Seung Soo Lee,[†] Minjung Cho,[†] Andrew Ozarowski,[∥] Arjun Prakash,[†] J. T. Mayo,[†] Cafer Yavuz,[†] and Vicki. L. Colvin*[,†]

[†]Department of Chemistry, Rice University, MS 60, Houston, Texas 77005, United States

[‡]CSRRI-IIT, MRCAT, Advanced Photon Source, Argonne National Laboratory, 9700 S. Cass Avenue, Argonne, Illinois 60439, United States

[§]Physics Department, Illinois Institute of Technology, Chicago, Illinois 60616, United States

[∥]National High Magnetic Field Laboratory, Florida State University, 1800 E. Paul Dirac Drive, Tallahassee, Florida 32310, United States

Supporting Information

ABSTRACT: Iron oxide nanocrystals are of great scientific and technological interest. In this work, these materials are the starting point for producing a reactive nanoparticle whose surface resembles that of natural green rusts. Treatment of iron oxide nanoparticles with cysteamine leads to the reduction of iron and the formation of a brilliant green aqueous solution of nanocrystals rich in iron(II). These materials remained crystalline with magnetic and structural features of the original iron oxide. However, new low-angle X-ray diffraction peaks as well as vibrational features characteristic of cysteamine were found in the nanocrystalline product. X-ray absorption spectroscopy (XAS), X-ray photoemission (XPS) and Mössbauer spectroscopies indicated the presence of an iron(II)-rich phase with high sulfur content analogous to the iron−oxygen structures found in natural green rusts. Electron microscopy found that these structural components remained associated with the nonreduced iron oxide cores. These sulfur-rich analogs of natural green rusts are highly reactive and were able to rapidly degrade a model organic dye in water. This observation suggests possible actuation with a cysteamine treatment of inert and magnetic iron oxide particles at the point-of-use for environmental remediation.

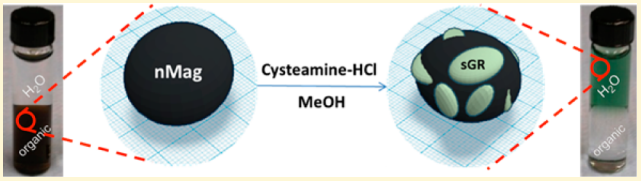

INTRODUCTION

Reactive nanoparticles, particularly formed from reduced iron phases, have found wide application in environmental remediation. The most reactive of these are the fully reduced "zero valent iron" nanoparticles; as the iron oxidizes in water, these can remove dyes from water, as well as dechlorinate halogenated contaminants.[1,2] Field trials of these materials have illustrated the value of this in situ alternative to the pump-and-treat paradigm for treating heavily contaminated water. Alternatively, high surface area green rusts have also been applied as reactive sorbents for the removal of nitrate, disinfection byproducts, and radioactive wastes such as technetium.[3−5] These materials also have high levels of iron(II) in their iron-oxyhydroxide layers and offer the potential for intercalating anionic contaminants.[6−8] Finally, reduced iron oxides, such as magnetite, can also dechlorinate carbon tetrachloride,[9−12] activate sulfate oxidation,[13] and promote uranium adsorption.[14−16] These examples illustrate that reduced iron can be a reactive agent when associated with nanostructured materials.

There are several established approaches for forming reduced iron nanoparticles. In the case of zerovalent iron nanoparticles, iron(III) salts can be reduced by borohydride in water under vigorous mixing.[17] Alternatively, reduced iron oxide particles may be formed in coprecipitation routes where iron salts are moderately reduced by ammonia.[18] Green rusts can also be formed by coprecipitation of iron salts as well as biologically mediated reduction of oxidized iron.[19,20]

In all cases, the final nanoparticles are generally not monodisperse or tunable in diameter. Additionally, they are formed in their most reactive state. This presents challenges for handling and storage, not to mention the poor control over particle size and morphology from the aqueous synthesis. Unfortunately, routes to more monodisperse nanocrystals occur at high temperatures in organic solutions under conditions that do not easily favor the reductive environments necessary to form iron(II); until recently, only iron(II)-rich nanoparticles with a core/shell of wüstite/magnetite were reported.[21]

The goal of this work was to examine the possibility of forming reduced iron(II) using monodisperse iron oxide nanocrystals, herein termed "nMag," as a starting material.

Received: August 6, 2014
Revised: October 27, 2014
Published: October 28, 2014

DOI: 10.1021/cm5028942
Chem. Mater. 2015, 27, 700−707

Strong reductants, such as borohydride, can dissolve particles. We reasoned that weaker reductants, such as organic thiols might be a better choice particularly for preserving the nanoparticle form. If this could be applied to highly uniform nanoscale iron oxides, it would represent a novel approach to forming reactive iron(II)-rich nanoparticles. Additionally, such treatments could make it possible to transform a relatively inert nanocrystal at the point of use into a reactive material thereby minimizing the challenges of storage. If the reduction were only at the surface, then the magnetic and oxidized core could allow for magnetic separation to be used to remove and possibly recycle materials.

Here, we report for the first time the synthesis of a novel and reactive iron-sulfide green rust from iron oxide nanocrystals. Thiol-containing amines reduced the surface of iron oxides nanocrystals, forming a brilliant green suspension of nanocrystals that were easily dispersed in polar solvents and water. Electron microscopy and X-ray diffraction revealed two phases present in the products arranged in a heterogeneous core/shell-like configuration (Scheme 1). The core remained identical to the starting iron oxide. The surface, however, was a nonuniform layered iron-sulfide that resembled iron-oxyhydroxide green rusts. This previously unidentified phase was characterized using X-ray diffraction, Mössbauer spectroscopy, vibrational spectroscopies, and X-ray absorption spectroscopies. As expected for this sulfur analog of a green rust, the material was able to remove a common dye from aqueous suspensions.

Scheme 1. Representation of the Sulfide Green Rust Formation and Proposed Chemical Structure[a]

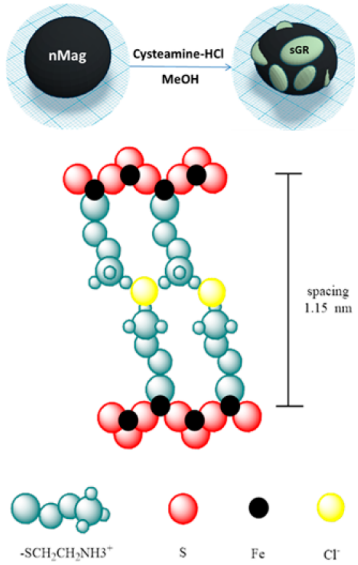

[a](Top) After treatment with cysteamine, the iron oxide nanoparticles show corrosion and are covered with non-uniform sulfide green rust (sGR) patches. (Bottom) Proposed chemical structure of sGR, which consists of cysteamine-intercalated layers of iron sulfur.

EXPERIMENTAL SECTION

Synthesis of Iron Oxide Nanocrystals. Iron oxide nanocrystals were made through established literature methods that form crystalline iron oxide through the thermal decomposition (T = 320 °C) of iron carboxylate intermediates in mixtures of oleic acid (OA) and octadecene (ODE).[22] The resulting solutions were provided in hexanes and appear dark brown to reddish depending on the iron concentration and reaction conditions. These iron oxide nanocrystal solutions were purified to remove unreacted oleic acid and other byproducts of the nanocrystal formation reaction. Using an autopipette (Eppendorf), 4 mL of the solutions were transferred into a 50 mL centrifuge vial; 4 mL each of methanol then acetone (EMD, 99.9%; EMD, 99.8%) were added and the resulting suspension centrifuged at 4,500 rpm for 30 min (Thermoscientific Sorvall Legend RT+ Centrifuge). This resulted in a dark brown or black pellet along with a clear or sometimes pale yellow supernatant; in some cases, this process was repeated to ensure the complete removal of any impurities. After disposing of the supernatant, we again redispersed the pellet in 4 mL of hexanes (Fisher, 99.8%); dispersion was readily observed after the tube was shaken with a Scientific Industries Vortex Genie 2-T vial shaker at the lowest setting for 10 min. This yielded a clear and brownish or red solution which was generally subjected to several more centrifugation and redispersion cycles. The purification process was complete once a clear supernatant was observed. In the final purification step, the nanoparticle pellet was redispersed in ODE (Sigma, 90%). Brief probe sonication (Dr. Hielscher Up100h Ultrasonic Processor) for about 1−3 s may be required to help solubilize the pellet in ODE.

Sulfide Green Rust Reaction. First, 0.56 mL of the nanocrystal solution in hexanes was dispensed into a 2 mL centrifuge vial. An equivalent volume of ODE was then added, and the solution was mixed via a few seconds-long bath sonications (FS6 sonicator from Fischer Scientific). Next, 0.44 mL of a 2.0 M solution of aminoethanethiol HCl (Sigma, 98%) in methanol (EMD, 99.8%) was added to the reaction vial to obtain a reactant/Fe ratio of 30 (increasing the ratio can induce aggregation; decreasing the ratio precludes any reaction). This solution, which appeared increasingly green and cloudy, was shaken for 3 h with an Eppendorf Minispin at 1100 rpm. A dark green precipitate formed during this time. Then, 1 mL of ultrapure water (Millipore, 18.2 MΩcm) was added to the solution and briefly shaken by hand to full dispersion, followed by 1 mL each of ethanol then ether (Decon Laboratories, 200 proof; Fisher, 99.9%). This mixture was shaken well by hand and then centrifuged at 4500 rpm for 30 min, forming a very dark green supernatant and pellet. The supernatant was decanted, and the pellet was saved. One milliliter (1 mL) each of ultrapure water, ether, then ethanol was added again, and the purification was repeated several more times, reserving subsequent pellets and purifying them. The resulting samples were inverted onto a paper towel for 5−10 min to dry and aid removal of any other leftover reactants and organics. The green solids were easily redispersed in 0.1−1 mL ultrapure water, although a brief 1−3 s bath sonication was sometimes applied. Upon visual inspection, we observed that the solutions were a brilliant and clear emerald green. Immediate storage under inert atmosphere allowed for the material to remain stable for further analysis; however, storage periods longer than 24 h resulted in oxidation of the iron(II).

Orange II Dye Remediation Tests. Dye samples were prepared by mixing 10 μL of sGR/Fe_xO_y with 15 μL of the azo group-containing Orange II dye (Acid Orange 7; Aldrich, CAS 633-95-5) and diluting the mixture with 1.975 mL of water. Five increasing concentrations of dye were prepared and used in triplicate. Standards were also prepared in triplicate with 15 μL of dye and 1985 μL of water. The solutions and standard were then mixed and filtered through a 0.22 μm syringe filter (Millipore, Millex-GP poly(ether sulfone), PES) to remove the sulfide-GR/Fe_xO_y. UV−vis spectroscopy was then used to determine the concentration of dye and determine when no further reaction occurred; additional experiments over several weeks found no change in these observations.

Sulfide Green Rust Reaction, Without Nanoparticles. This material was required for analysis of some of the X-ray absorption data. The synthetic route is identical, except that instead of using nanoparticles, an equimolar amount of iron oleate served as the iron source.

Preparation of Iron Oleate. Iron oleate was prepared by combining hydrated iron oxide (FeOOH, catalyst grade, 30−50 mesh; 1 mmol, 0.09 g), oleic acid (OA, technical grade, 90%; 4 mmol, 1.12 g) and 1-octadecene (ODE, technical grade, 90%; 15 mmol, ~ 4

DOI: 10.1021/cm5028942
Chem. Mater. 2015, 27, 700−707

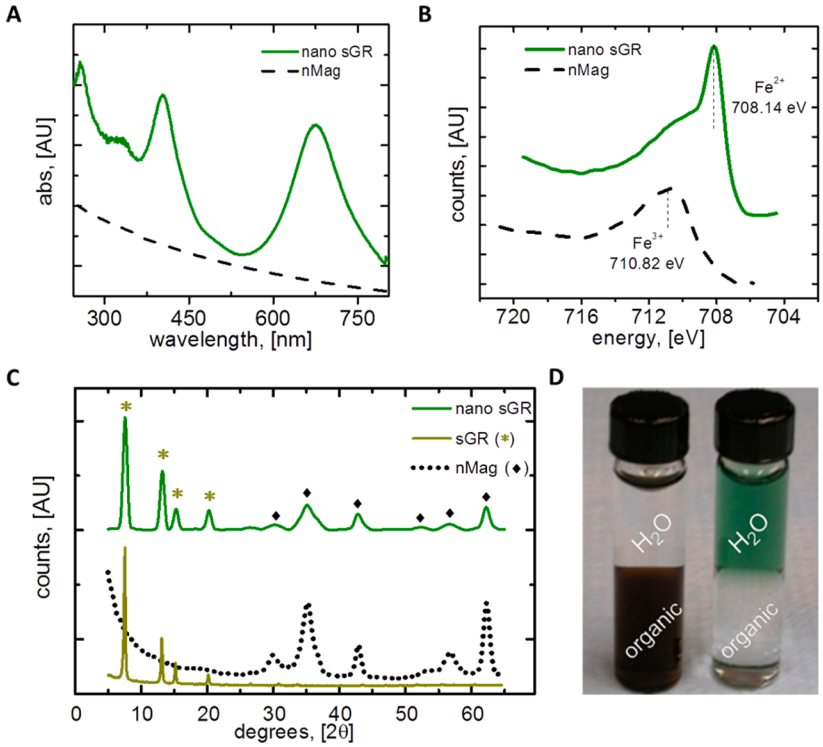

Figure 1. Sulfide green rust (sGR) was easily formed using an intercalated cysteamine-HCl and nanocrystalline iron oxide precursor. (a, dashed line) Nanocrystalline iron oxide was initially prepared in the organic phase and colored brown due to a lack of absorbance peaks in the UV−vis. (a, solid line) After the sulfide green rust synthesis, a brilliant green color was readily apparent; major optical absorbance peaks were present at 400 and 675 nm, corresponding to adsorption peaks in the red and blue range. (b) An increase of Fe^{2+}coincided from the synthesis as observed by Fe $2p_{3/2}$XPS. This reduced iron state was the result of a reaction with sulfur in the cysteamine with nanocrystalline iron oxide, producing (c) a unique XRD spectrum with low 2θ peaks. Magnetite persists after the reaction, as the diffraction pattern for both the sGR and nanocrystalline iron oxide are visible. (d) Transfer from the organic to the aqueous phase was total after synthesis.

g) and heating the mixture at 240 °C for 1 h. The resulting black precipitate was purified using acetone, methanol, and hexanes. Five milliliters (5 mL) of the resulting precipitate was washed using 25 mL of acetone and 25 mL of methanol and centrifuged at 4500 rpm for 30 min. The purification was repeated three times, and then the black solid was dissolved in 15 mL of hexanes. The Fe concentration was measured by ICP-AES to be 3 mg/mL.

Extended X-ray Absorption Fine Spectroscopy (EXAFS). EXAFS measurements were done at the MRCAT 10-ID beamline at the Advanced Photon Source, Argonne National Laboratory.[23] EXAFS was done at the Fe K edge (7112 eV). Samples were mounted in plexiglass sample holders (5 mm diameter and 0.2 mm thick) for the fluorescence measurements. The iron standards needed for this experiment ($FeCl_3$, FeS_2, and Fe metal foil) were measured in transmission mode. The powders were spread on kapton tape and several layers were stacked so that the thickness (x) of the samples corresponded to $\Delta\mu x$ = 0.5, where $\Delta\mu$ is the edge step of the absorption coefficient at the Fe K-edge energy. Both for transmission and fluorescence measurements with ionization chambers, the Si(111) double crystal monochromator was scanned continuously so that the data was collected in quick EXAFS mode. Ten EXAFS scans were taken and then averaged for the liquid sample. The undulator parameters (taper and gap) were optimized to obtain a large photon flux with nearly constant intensity within the scanned energy range of 6900−8100 eV for the Fe edge. Scans were taken from −200 eV below Fe edge (7112 eV) to 900 eV above fe edge with step size of 0.3 eV and scanning time used was 0.1 s per point. An Rh harmonic rejection mirror was used to eliminate X-rays of higher harmonic energies. The incident ion chamber was filled with 20% nitrogen mixed with 80% helium gas, whereas the transmission ion chamber was filled with nitrogen gas for proper adsorption. A reference ion chamber filled with the same gases as the transmission ion chamber was mounted behind the latter so as to record a standard spectrum of Fe foil with every scan to ensure that there is no energy shift between each scan. For fluorescence measurements, the Lytle detector was filled with argon gas. The size of the incident X-ray beam on the sample was 300 × 300 μm. The data was processed using Athena by extracting the XAFS oscillations χ(k) as a function of photoelectron wavenumber k following standard procedures.[24] The theoretical paths were generated using FEFF6 and the models were done in the conventional way using the fitting program called Artemis.[25,26] Artemis was used to refine the fitting parameters used for modeling each sample in R-space until a satisfactory model describing the system was obtained. Data sets were simultaneously fitted in R-space with k-weights of 1, 2, and 3.

X-ray Diffraction (XRD). XRD spectra were collected on a Rigaku D/Max Ultima II Powder Diffratometer. Solid sulfide green rust (sGR)/nanocrystalline iron oxide powder samples were deposited onto a round, 5 mm diameter × 0.2 mm deep indented Rigaku zero-background holder. The sample was then scanned for 5 h with the following settings: 0.5° 2θ divergence and scattering slits, a 10 mm divergence height limiting slit, a 0.15 mm receiving slit, a 0.1° 2θ step size, and a 21.1 s/step rate. Jade 9.0 was then used to analyze the resulting spectrum.

UV−Vis Spectroscopy. UV−vis spectroscopy was carried out using a Varian Cary 5000i UV−vis-NIR Spectrophotometer. Twenty microliters (20 μL) of the sulfide GR solution was added to 0.98 mL of water. This solution was then placed inside the spectrometer measuring a range of 225 to 800 nm. The measurement speed was 600 nm/min.

X-ray Photoelectron Spectroscopy (XPS). XPS was carried out on a PHI Quantera XPS using a substrate of indium foil at 140 eV (low resolution) for survey scans and 26 eV (high resolution) for elemental scans. One hour before introduction into the sample chamber, 0.15 μL of sample was dropped onto the substrate. All scans utilized electron and ion neutralizers. Using PHI Multipak 7.0, the

DOI: 10.1021/cm5028942
Chem. Mater. 2015, 27, 700−707

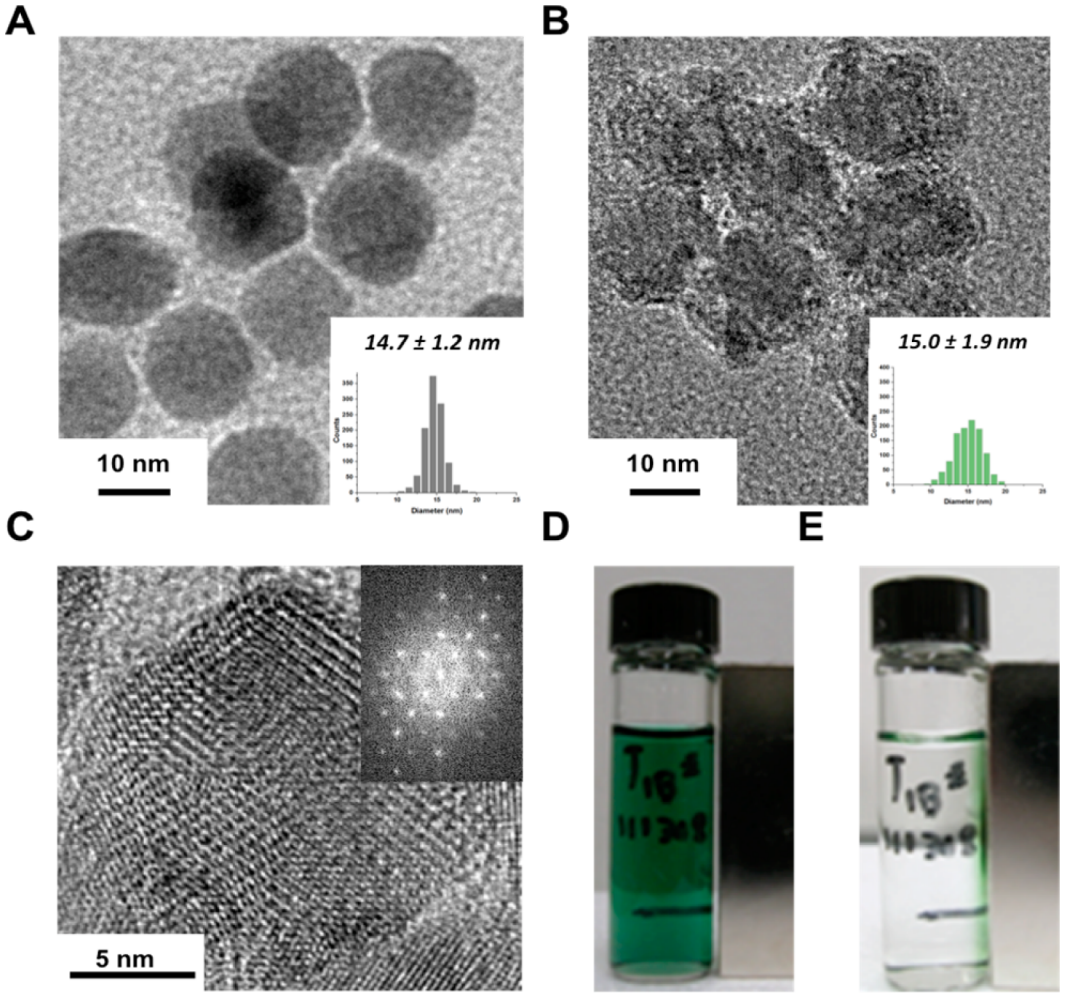

Figure 2. Sulfide green rust was associated with unreacted nanocrystalline iron oxide, and the physical properties of the nanocrystalline iron oxide were retained. Nanoparticle size was conserved, as seen by TEM (a) before (b) and after the sGR synthesis, with size changing within standard deviation. Over 1000 particles were counted to be statistically accurate. (a) Typical magnetite nanoparticles obtained (b) a more corroded particle surface after the reaction. (c) High-resolution imaging and (c, inset) corresponding power spectrum confirmed the crystallinity of the final product and the existence of a larger *d*-spacing that corroborates well with X-ray diffraction data. (d and e) Nanocrystalline iron oxide's magnetic properties were preserved, as a hand-held neodymium magnet was observed to remove the nano sGR within 24 h.

spectrum was corrected using the adventitious carbon peak (284.5 eV), and peak multiplets were assigned.

High-Resolution Transmission Electron Microscopy (HRTEM). TEM images were obtained using a JEOL 2100 Field Emission Gun TEM at 200 kV with a single-tilt sample holder using 400 mesh ultrathin carbon-A type copper grids from Ted Pella, Inc. Energy-filtering TEM (EFTEM), along with Gatan imaging filter (GIF) mapping and energy-dispersive X-ray spectrometry (EDXS), provided the chemical composition information for the complexes observed.

Sizing images were acquired via a JEOL 1230 High-Contrast Transmission Election Microscope at 80 kV with a single-tilt multisample holder using the same grid type. About an hour before use of the machine, 150 μL of sample was dried onto the grid. Image interpretation and sizing calculations were obtained by counting over 1000 individual nanocrystalline particles using Media Cybernetics ImagePro Plus 5.0.

Mössbauer Spectroscopy. Data was collected via a SeeCo (Edina, MN) instrument. Samples were deposited onto kapton film and sealed together for measurement. Spectra were then recorded with constant acceleration mode at 77 K. Final data was both smoothed and calibrated versus an α-iron foil standard.

Raman Spectroscopy. Raman spectroscopy was carried out on a Renishaw InVia Raman Microscope using a 633 nm laser with a 1800 lines/mm filter. Around 0.25 mL of sample was dropped onto a glass slide and allowed to dry over the course of a few hours. Spectra were taken using a 50× lens with the laser set at 50% power for 20 s and averaged over three scans.

Infrared Spectroscopy. Infrared spectra were collected in a Jasco FT-IR 660 Plus Spectrometer using an ATR setup with a diamond substrate. One hundred microliters (100 μL) of the sample solution were dried on to the cleaned substrate and blown with nitrogen for 30 min to purge interferences. Spectra were run with a resolution of 4 cm^{-1} with averaging over 16 scans.

■ RESULTS AND DISCUSSION

A novel nanoscale iron sulfide compound, termed here "sulfide green rust" or sGR, was formed by treating nanocrystalline iron oxides with cysteamine. Iron-thiol chemistry is central to this reaction, specifically the reaction of sulfur from the cysteamine with iron from the nanocrystalline iron oxide. Similar chemistry has been observed from bulk starting materials, but the product was not water-soluble or green.[27] Briefly, an alcoholic solution of cysteamine hydrochloride, a known metal ion scavenger, was added to an organic dispersion of nanocrystalline iron oxide.[28,29] After 2−3 h of mixing in a sealed vial, a green color was observed in the alcoholic phase, and the organic

DOI: 10.1021/cm5028942
Chem. Mater. 2015, 27, 700−707

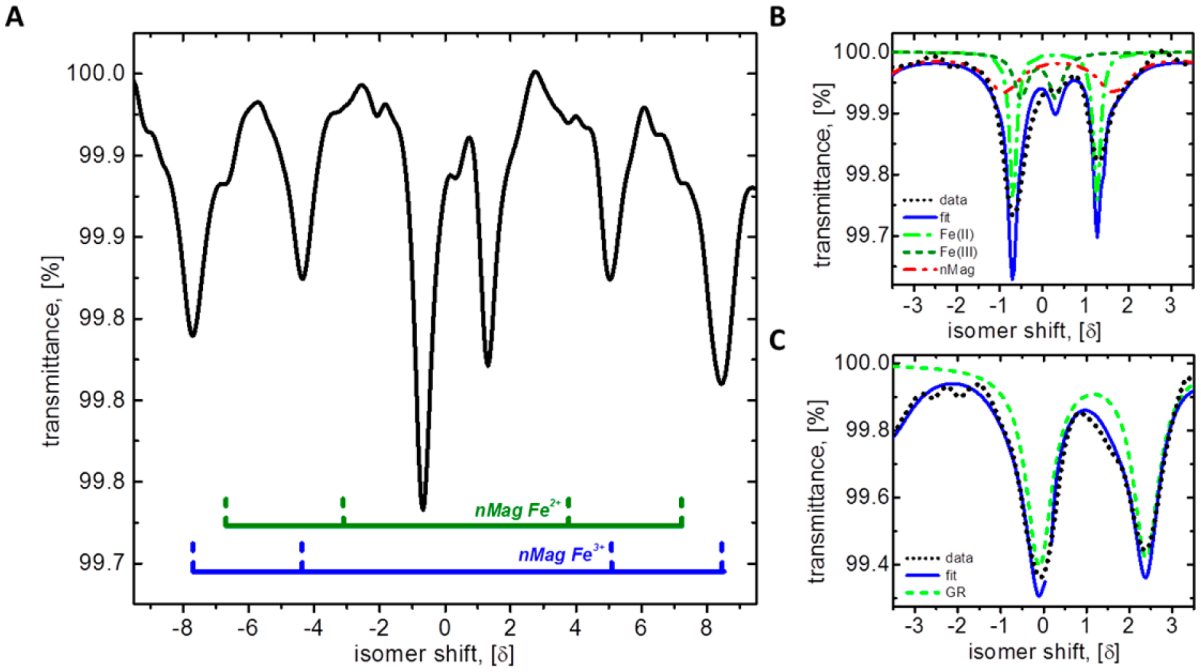

Figure 3. Both sulfide green rust and magnetite were still present after complexation. (a) The 77K Mössbauer spectrum of nano sGR illustrates two phases: the multiple overlapping sextets related to magnetite and two doublets assigned to sGR. Magnetite's two resulting sextets are indicative of Fe^{2+} and Fe^{3+} typical of magnetite below the Verwey transition. (b) Isomer shifts (δ) of 0.147 mm/sec for the sGR were similar to iron sulfide minerals such the Fe(II) in bulk FeS_2 marcasite (δ = 0.149 mm/sec), and certain iron dithiolates (δ = 0.15 mm/sec); quadrupole splitting (QS) of 1.98 mm/sec for the sGR suggests distortion possibly due to the large cysteamine molecule in the crystal structure or a better match for a dithiol. (c) Samples of GR-Cl were also were prepared and measured for comparison. Lack of the characteristic large isomer shift (δ = 1.1) and quadrupole splitting (QS = 2.2) observed in the GR-Cl confirmed that our sGR had a unique crystal structure and was not a classical green rust.

phase was nearly colorless. The optical absorbance of the aqueous sample showed two peaks at 400 and 675 nm (Figure 1A), which, taken together, proved to be a reliable, quick fingerprint for a successful reaction.

Therefore, during this process the brownish-black material, with no adsorption peaks in the visible spectra, was transferred from the organic phase to the aqueous phase, in which it appeared green (Figure 1D) with adsorption peaks in the blue and red spectra.

A variety of molecular and solid state characterization tools, described in the following sections, indicate that the cysteamine treatment forms an iron−sulfur phase on the nanocrystal surfaces (Scheme 1). This marcasite FeS_2-related material is clay-like, characterized by planar iron−sulfur layers separated by relatively large distances ($d \sim 11.5$ Å).

Cysteamine is an intercalant, and as shown in Scheme 1, two end-to-end molecules can account for the specific low angle *d*-spacing observed in X-ray diffraction.[30,31] This structure is analogous to green rusts in which reduced iron oxide layers intercalate basic anions; for that reason we term the product a "sulfide green rust".

An important feature of the final product is that it contains a reduced form of iron. The green color of the product (Figure 1) suggests the presence of iron(II) and this was verified by XPS.[32,33] Figure 1B shows the Fe $2p_{3/2}$ XPS spectra of the starting iron oxide compared to the green product. A clear change in the iron oxidation state was evident after treatment with cysteamine: the iron peak position shifts from 710.82 eV (Fe(III)) to 708.14 eV (Fe(II)).[33,34] After several days of exposure to air, the Fe(II) oxidized back to Fe(III) with a corresponding shift in XPS features and in color (Supporting Information, SI Figure 1). These XPS results are not surprising because thiols have been shown to reduce iron(III) to iron(II) in water.[35] This effect has been observed with other anions,[36] and previous studies have shown this to occur via electron transfer from the sulfur to the iron.[35]

The final product also consists of two distinct crystallographic phases (Figure 1C). The X-ray diffraction data indicate that crystalline iron oxide is present both before and after the treatment. We refer to this initial phase as "iron oxide" or Fe_xO_y because it is not straightforward to distinguish between magnetite and maghemite starting materials using only X-ray diffraction.[37,38] After treatment with the cysteamine, new diffraction peaks are clearly visible at 7.69°, 13.2°, 15.37°, and 20.21°. The new pattern did not match to any known phase in either JADE or online RRUFF crystallographic databases (Supporting Information, SI Table 1).

The strongest feature was a low 2θ peak at 7.69° corresponding to a 11.5 Å *d*-spacing. Iron-containing clays such as those found in loess soils (e.g., smecite group) frequently are identified by these low-angle peaks, which arise from the Fe-rich layers that intercalate anions as large as 10 Å.[39] Of particular interest are green rusts, which may incorporate large organic anions such as lactates, giving rise to *d*-spacings in excess of 10 Å (e.g., 14.8 nm and 44.4 Å, respectively).[30,40] We note that after thermal treatment above the melting point of cysteamine, this low-angle peak disappeared (Supporting Information, SI Figure 2).[28] The presence of cysteamine was also confirmed via both Raman and infrared spectroscopy (Supporting Information, SI Figures 3 and 4 and SI Table 2)

We evaluated whether this new phase was physically associated with the nanocrystalline magnetite using both electron microscopy and magnetic separation. Low-magnification images show that nanocrystals are present in the green

DOI: 10.1021/cm5028942
Chem. Mater. 2015, 27, 700−707

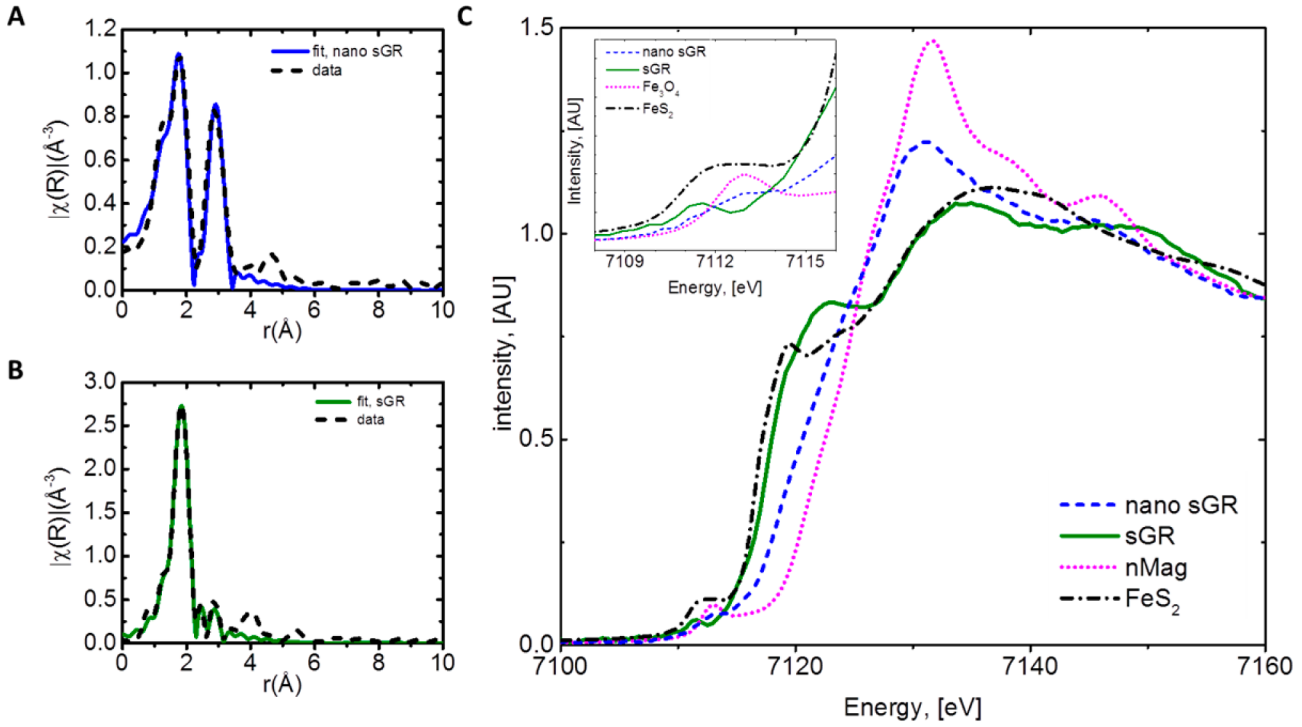

Figure 4. Sulfide green rust was composed of Fe−S bonds similar to the iron sulfide mineral, marcasite. (a) Fe K-edge EXAFS magnitude FT data demonstrated both sulfur and oxygen atoms bound to iron. Fitting included contributions of Fe−S at 2.24 Å (bulk marcasite FeS_2, 2.26 Å), Fe−Fe at 3.41 Å (bulk marcasite FeS_2, 3.82 Å), and Fe−O at 1.86 Å (magnetite Fe_3O_4, 1.89 Å) with a good R-factor fit of 0.03. (b) Control experiments were also conducted on a homogeneous sample synthesized from dissolved iron, with contributions only from sulfur resulting; the atomic distances for Fe−S and Fe−Fe were 2.29 and 3.41 Å, respectively (see Supporting Information for details). (c) Fe K-edge XANES spectra of the sGR compared standard compounds containing Fe in various oxidation states and geometries further corroborated a good match for Fe−S bonding and (c, inset) indicated a general increase in Fe(II) from precursor nMag levels.

product solutions, and this is consistent with the X-ray diffraction of the solid product (Figure 2A,B). Analysis of over a thousand particles yields a particle size distribution very similar to the starting material, Fe_xO_y (Figure 2A,B insets); however, the surfaces of cysteamine treated particles appear more heterogeneous under higher magnification (Figures 2B). Figure 2C shows a HRTEM image of a cysteamine-treated nanoparticle with its corresponding power spectrum or FFT. From these, we determined that the nanoparticles are pollycrystalline and confirmed the coincidence of a large *d*-spacing (11.5 Å) characteristic of green rusts which corroborate the *d*-spacings calculated from the low-angle peaks of the XRD spectra (Supporting Information, SI Table 3). Analytical electron microscopy of this product also revealed sulfur to be present at the nanocrystal interface (Supporting Information, SI Figure 5).

Additionally, the green product could be removed from solution using a hand-held neodymium magnet (Figure 2D,E). Because iron clays are not generally magnetic, this behavior is consistent with a structural model in which the cysteamine reacts with surface iron, resulting in a new phase that remains physically associated with the nanocrystal Fe_xO_y cores.[41]

To better evaluate the physical structure associated with the modified iron oxides, we employed Mössbauer spectroscopy to examine the iron environments. The signature spectrum of nanocrystalline iron oxide is illustrated in Figure 3A, featuring two main sextets related to Fe^{2+} and Fe^{3+} below the Verwey transition.[37] A separate phase consisting of two doublets was observed near the center of the spectrum (Figure 3B). Mössbauer isomer shifts (δ) of 0.147 mm/sec show close matches to the FeS_2 pyrite dimorph marcasite (δ = 0.149 mm/sec), as well as a close match to iron dithiolates (δ = 0.15 mm/sec).[42,43] Quadrupole splitting (QS) of 1.98 mm/sec was much higher than literature values for marcasite (QS = 0.504); this could be due to distortion caused by the large organic ligand in the crystal structure or possibly a closer match to the iron dithiolate (QS = 1.98). The second doublet observed for the green product was assigned to an oxidized Fe(III) derived from the iron−sulfur phase. Neither of these peaks have either the isomer shifts or quadrupole splitting characteristic of either synthetic and natural green rusts (Figure 3C).[44] Conventional green rust has iron−oxygen layers; our Mössbauer data suggests that in this structure iron is bonded predominantly to sulfur.

Additional confirmation of iron−sulfur bonding can be seen via Fe K-edge X-ray absorption measurements (Figure 4A). A critical first step for analyzing multiple phases in EXAFS data is to acquire calibration materials, which are pure single phases. This was straightforward for the iron oxide component, as the unreacted nanocrystalline iron oxide was readily available. However, forming the iron−sulfur clay phase required a reaction that mimicked our cysteamine treatment without the nanocrystals. To that end, we found that if we treated the precursor to the nanocrystal, iron oleate, with cysteamine in methanol, then it was possible to generate a green product (sGR) with identical major X-ray diffraction features to that of the nano sGR seen in Figure 1C. Using this pure phase, it was possible to assign the features in the X-ray absorption spectrum (Figure 4).

Shown compared to the data is a fit that assumes 2.24 Å for Fe−S, 3.40 Å for Fe−Fe, and 1.86 Å Fe−O with an excellent R-

DOI: 10.1021/cm5028942
Chem. Mater. 2015, 27, 700−707

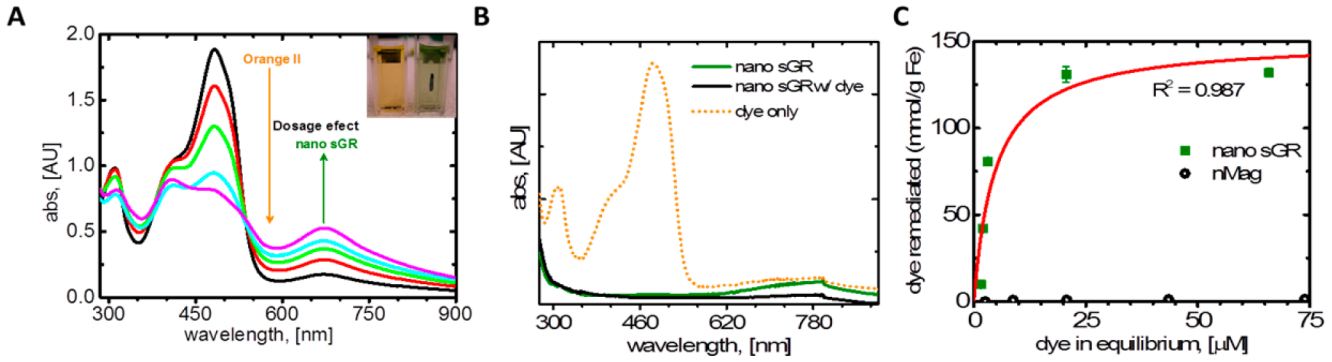

Figure 5. Sulfide green rust has potential for use. (a) Remediation of an azo dye was observed via UV−vis with fast reaction rates at different dosages of nano sGR, (a, inset) also observable to the naked eye. (b) Controls tested the sample filtrate after passing only dye, only nano sGR, and nano sGR added to dye through a 0.22 μm PES membrane filter; no color was present in the samples after each filtration in both cases when nano sGR is filtrated. (c) A quantitative analysis was made at several concentrations of Orange II; remediation performance by nano sGR is more than 100 times greater than its precursor nMag.

factor (0.03; 0.05) is the maximum allowed value for a good fit; also, we note that the second phase matched very closely to typical Fe_xO_y iron oxide, with an Fe−O bond distance of 1.89 Å. Contributions of Fe−S and Fe−Fe are from the sGR, with the additions of Fe−O generated from nanocrystalline iron oxide (Supporting Information, SI Table 4). Peaks found at 2.29 and 3.41 Å using our control phase further confirm our model with an R-factor fit of 0.01 (Figure 4B). For comparison, marcasite, the compound that matched well to the Mössbauer data, was run on EXAFS with strikingly similar results for Fe−S (2.26 Å) and Fe−Fe (3.82 Å) distances. Conversely, fits for other green iron complexes with hypothetical Fe−Cl or Fe−O bonds were poor; visual inspection of XANES data also suggests a better match to Fe−S (Figure 4C). Further details on XAS measurements can be found in the Supporting Information (SI Figure 6).

Taken together, the data indicate that the cysteamine treatment produces a clay-like iron-sulfide material at the nanocrystal interface (Scheme 1). WE refer to it here as "sulfide green rust" or sGR to distinguish it from green rusts that possess iron−oxygen frameworks. The material is a layered structure with alternating planes of marcasite-like Fe centers that intercalate cysteamine molecules. Simple energy minimization exercises via ChemDraw (not shown) illustrated that two cysteamines stacked as shown in Scheme 1 provide a *d*-spacing comparable to that observed. This chemistry occurs at the surface of the iron oxide nanocrystals and enriches the material with reactive iron(II). Such a feature combined with the ability to recover the materials via membrane filtration or magnetic separation suggests some promise as agents for environmental remediation.

To evaluate whether this material had any reactivity to organic compounds, we compared this nanoscale sGR against bilayer-coated, water-soluble nanocrystalline iron oxide—the initial reagent in the formation of nano sGR—for the chemical degradation of a water-soluble dye. For a model system, we chose the potential mutagenic dye Orange II, which has an azo functional group used in GR studies as a benchmark for contaminant remediation.[45] The nano sGR easily degraded the dye as measured by the disappearance of key absorbance features as the dosage was increased (Figure 5A). After filtration through a 0.22 μm PES membrane syringe filter, all of the green material and dye was removed from the solution when nano sGR is added, as observed via UV−vis analysis. The opposite is observed when only dye is filtered; the soluble azo dye is not retained by the filter (Figure 5B). Perhaps due to the extent of iron(III) reduced in the new material, sGR performed quite well. After fitting the amount of remediation to a Langmuir model (assuming a surface interaction), the maximum remediation capacity found was 150 mmol/g Fe, which corresponds to the remediation of 8.4 mol of dye by mol of iron. Contrasting, there was no comparable change in the dye exposed only to the nanocrystalline magnetite (Supporting Information, SI Figure 7), which confirms that the application capability comes from the sGR phase, and it is not present in the precursor.

■ CONCLUSIONS

A green iron sulfide can be synthesized around nanocrystalline iron oxide cores. EXAFS and Mössbauer analyses both indicate the existence of Fe−S bonds. X-ray diffraction finds large *d*-spacings consistent with a layered type of material. Synthesis of this sulfide green rust is simple, fast, and utilizes the organothiol cysteamine as a reductant; the result is a material with reactive properties due to a high iron(II) content. The sulfide green rust is associated with the nanoparticle, making it possible for the iron oxide nanocrystal to serve as a "scaffold" for reactive chemistry. Potential applications for the material match well with other reactive iron(II) compounds, including fast dye remediation. This enhanced reactivity suggests a useful material, perhaps utilizing its magnetic properties or including other typical iron sulfide applications such as corrosion alleviation, catalysis, or hydrotreating.[46,47]

■ ASSOCIATED CONTENT

Supporting Information

Time-lapse Fe XPS spectra of the sGR; high-temperature XRD; sGR XRD 2θ listings; Raman and infrared spectroscopies; GIF TEM elemental mapping; fitting paths for EXAFS calculations; and tables for Raman, FFT, and XAS assignments and calculations. This material is available free of charge via the Internet at http://pubs.acs.org.

■ AUTHOR INFORMATION

Corresponding Author

*Tel: (713) 348-5741. Fax: (713) 348-2578. E-mail: colvin@rice.edu.

DOI: 10.1021/cm5028942
Chem. Mater. 2015, 27, 700−707

Notes

The authors declare no competing financial interest.

■ ACKNOWLEDGMENTS

S.C. would like to thank Dr. Tomohiro Shibata of the Illinois Institute of Technology; Dr. Shelly D. Kelly of EXAFS Analysis, Inc. for discussions and help during the EXAFS measurements and analysis of EXAFS data; and Dr. Vladislav Zyranov for his help in making the necessary sample holders for the experiments. MRCAT operations are supported by the Department of Energy and the MRCAT member institutions. Use of the Advanced Photon Source at Argonne National Laboratory is supported by the U.S. Department of Energy, Office of Science, Office of Basic Energy Sciences, under Contract No. DE-AC02-06CH11357.

■ REFERENCES

(1) Lin, Y. T.; Weng, C. H.; Chen, F. Y. *Sep. Purif. Technol.* **2008**, *64*, 26.
(2) Liu, Y. Q.; Majetich, S. A.; Tilton, R. D.; Sholl, D. S.; Lowry, G. V. *Environ. Sci. Technol.* **2005**, *39*, 1338.
(3) Choi, J.; Batchelor, B. *Chemosphere* **2008**, *70*, 1108.
(4) Chun, C. L.; Hozalski, R. M.; Arnold, W. A. *Environ. Sci. Technol.* **2007**, *41*, 1615.
(5) Pepper, S. E.; Bunker, D. J.; Bryan, N. D.; Livens, F. R.; Charnock, J. M.; Pattrick, R. A. D.; Collison, D. *J. Colloid Interface Sci.* **2003**, *268*, 408.
(6) Bond, D. L.; Fendorf, S. *Environ. Sci. Technol.* **2003**, *37*, 2750.
(7) Skovbjerg, L. L.; Stipp, S. L. S.; Utsunomiya, S.; Ewing, R. C. *Geochim. Cosmochim. Acta* **2006**, *70*, 3582.
(8) Hanna, K.; Kone, T.; Ruby, C. *Environ. Sci. Pollut. Res.* **2010**, *17*, 124.
(9) Amonette, J. E.; Workman, D. J.; Kennedy, D. W.; Fruchter, J. S.; Gorby, Y. A. *Environ. Sci. Technol.* **2000**, *34*, 4606.
(10) Elsner, M.; Schwarzenbach, R. P.; Haderlein, S. B. *Environ. Sci. Technol.* **2004**, *38*, 799.
(11) Gorski, C. A.; Nurmi, J. T.; Tratnyek, P. G.; Hofstetter, T. B.; Scherer, M. M. *Environ. Sci. Technol.* **2010**, *44*, 55.
(12) Ayala-Luis, K. B.; Cooper, N. G. A.; Koch, C. B.; Hansen, H. C. B. *Environ. Sci. Technol.* **2012**, *46*, 4683.
(13) Fang, G. D.; Dionysiou, D. D.; Al-Abed, S. R.; Zhou, D. M. *Appl. Catal., B* **2013**, *129*, 325.
(14) Latta, D. E.; Gorski, C. A.; Boyanov, M. I.; O'Loughlin, E. J.; Kemner, K. M.; Scherer, M. M. *Environ. Sci. Technol.* **2012**, *46*, 778.
(15) Duff, M. C.; Coughlin, J. U.; Hunter, D. B. *Geochim. Cosmochim. Acta* **2002**, *66*, 3533.
(16) Waite, T. D.; Davis, J. A.; Payne, T. E.; Waychunas, G. A.; Xu, N. *Geochim. Cosmochim. Acta* **1994**, *58*, 5465.
(17) Li, X.-Q.; Elliott, D. W.; Zhang, W.-X. *Crit. Rev. Solid State Mater. Sci.* **2006**, *31*, 111.
(18) Eivari, H. A.; Rahdar, A. *World Appl. Programming* **2013**, *3*, 52.
(19) Ona-Nguema, G.; Abdelmoula, M.; Jorand, F.; Benali, O.; Gehin, A.; Block, J. C.; Genin, J. M. R. *Environ. Sci. Technol.* **2002**, *36*, 16.
(20) Usman, M.; Hanna, K.; Abdelmoula, M.; Zegeye, A.; Faure, P.; Ruby, C. *Appl. Clay Sci.* **2012**, *64*, 38.
(21) Lak, A.; Kraken, M.; Ludwig, F.; Kornowski, A.; Eberbeck, D.; Sievers, S.; Litterst, F. J.; Weller, H.; Schilling, M. *Nanoscale* **2013**, *5*, 12286.
(22) Yu, W. W.; Falkner, J. C.; Yavuz, C. T.; Colvin, V. L. *Chem. Commun.* **2004**, 2306.
(23) Segre, C. U., et al. In *Synchrotron Radiation Instrumentation*, Proceedings of the 11th U.S. National Conference, *CP521*; American Institute of Physics: New York, 2000; pp 419−422.
(24) Newville, M. *J. Synchrotron Radiat.* **2001**, *8*, 322.
(25) Zabinsky, S. I.; Rehr, J. J.; Ankudinov, A.; Albers, R. C.; Eller, M. J. *Phys. Rev. B* **1995**, *52*, 2995.
(26) Ravel, B.; Newville, M. *J. Synchrotron Radiat.* **2005**, *12*, 537.
(27) Rickard, D.; Luther, G. W. *Chem. Rev.* **2007**, *107*, 514.
(28) Fleischer, H.; Dienes, Y.; Mathiasch, B.; Schmitt, V.; Schollmeyer, D. *Inorg. Chem.* **2005**, *44*, 8087.
(29) Gebremedhin-Haile, T.; Olguin, M. T.; Solache-Rios, M. *Water, Air, Soil Pollut.* **2003**, *148*, 179.
(30) Sabot, R.; Jeannin, M.; Gadouleau, M.; Guo, Q.; Sicre, E.; Refait, P. *Corros. Sci.* **2007**, *49*, 1610.
(31) Simon, L.; Francois, M.; Refait, P.; Renaudin, G.; Lelaurain, M.; Genin, J. M. R. *Solid State Sci.* **2003**, *5*, 327.
(32) Yoshioka, H. *J. Phys. Soc. Jpn.* **1949**, *4*, 270.
(33) Mullet, M.; Guillemin, Y.; Ruby, C. *J. Solid State Chem.* **2008**, *181*, 81.
(34) Mikhlin. *Geochim. Cosmochim. Acta* **2002**, *66*, 4057.
(35) Rao, T. V.; Sain, B.; Murthy, P. S.; Rao, T.; Jain, A. K.; Joshi, G. C. *J. Chem. Res., Synop.* **1997**, 300.
(36) Refait, P.; Drissi, S. H.; Pytkiewicz, J.; Génin, J. M. R. *Corros. Sci.* **1997**, *39*, 1699.
(37) Gorski, C. A.; Scherer, M. M. *Am. Mineral.* **2010**, *95*, 1017.
(38) Woo, K.; Hong, J.; Choi, S.; Lee, H. W.; Ahn, J. P.; Kim, C. S.; Lee, S. W. *Chem. Mater.* **2004**, *16*, 2814.
(39) Bishop, M., Hailiang, D., Jaisi, D., Ravi, K., Ji, J. Bioavailability of Fe(III) in Loess Sediments: An Important Source of Electron Acceptors. In Proceedings of *Clays of the Big Sky*: 46th Annual Meeting of The Clay Minerals Society, Billings, MT, June 5−11, 2009; Stucki, J. W., , Ed.; The Clay Minerals Society: Chantilly, VA, 2009; p 54.
(40) Ayala-Luis, K. B.; Koch, C. B.; Hansen, H. C. B. *Appl. Clay Sci.* **2010**, *48*, 334.
(41) Yavuz, C. T.; Mayo, J. T.; Yu, W. W.; Prakash, A.; Falkner, J. C.; Yean, S.; Cong, L. L.; Shipley, H. J.; Kan, A.; Tomson, M.; Natelson, D.; Colvin, V. L. *Science* **2006**, *314*, 964.
(42) Temperley, A. A.; Lefevre, H. W. *J. Phys. Chem. Solids* **1966**, *27*, 85.
(43) Blomquist, J.; Helgeson, U.; Folkesson, B.; Larsson, R. *Chem. Phys.* **1983**, *76*, 71.
(44) Genin, J. M. R.; Ruby, C. *Solid State Sci.* **2004**, *6*, 705−718
(45) Kone, T.; Hanna, K.; Abdelmoula, M.; Ruby, C.; Carteret, C. *Chemosphere* **2009**, *75*, 212.
(46) Stiefl, E. I. Transition Metal Sulfur Chemistry: Biological and Industrial Significance. In *Transition Metal Sulfur Chemistry*; Stiefel, E. I., Matsumoto, K., Eds.; ACS Symposium Series, Vol. *653*; The American Chemical Society: Washington, DC, 1996; pp 2−38.
(47) Rakowski DuBois, M.; Jagirdar, B.; Noll, B.; Dietz, S. Syntheses, Structures, and Reactions of Cyclopentadienyl Metal Complexes with Bridging Sulfur Ligands. In *Transition Metal Sulfur Chemistry*; Stiefel, E. I., Matsumoto, K., Eds.; ACS Symposium Series, Vol. *653*; The American Chemical Society: Washington, DC, 1996; pp 269−281.

DOI: 10.1021/cm5028942
Chem. Mater. 2015, 27, 700−707